



# Heat transfer enhancement in quasi-two-dimensional magnetohydrodynamic duct flows using repeated flow-facing wedge-shaped protrusions

Sneha Murali<sup>a,\*</sup>, Wisam K. Hussam<sup>b</sup>, Gregory J. Sheard<sup>a</sup>

<sup>a</sup> Department of Mechanical & Aerospace Engineering, Monash University, VIC 3800, Australia

<sup>b</sup> School of Engineering, Australian College Kuwait, Safat, Kuwait

## ARTICLE INFO

### Article history:

Received 17 December 2020

Revised 19 January 2021

Accepted 5 February 2021

### Keywords:

Quasi-two-dimensional MHD duct flows

Heat transfer enhancement

Surface modification

## ABSTRACT

Repeated flow-facing wedge-shaped protrusions are explored as a means to enhance the heat transfer behaviour in a quasi-two-dimensional magnetohydrodynamic duct flow. Quasi-two-dimensionality is achieved under a strong magnetic field which are prevalent in the cooling blankets of fusion reactors. Ranges of Hartmann friction parameters ( $50 \leq H \leq 500$ ) and Reynolds numbers ( $1300 \leq Re \leq 3000$ ) are investigated. The effect of blockage  $\beta$  (wedge height to duct height), pitch  $\gamma$  (distance between wedges) and wedge angle  $\phi$  on heat transfer ratio  $HR$  and efficiency  $\eta$  are considered. A monotonic increase in  $HR$  with  $\beta$  is observed in the range of  $\beta$  investigated. It is possible to further improve  $HR$  by changing the geometric parameter to an optimal pitch and optimal wedge angle. Corresponding to each  $H$  there exists an optimal  $\beta$ ,  $\gamma$  and  $\phi$  where maximum  $\eta$  could be achieved. In contrast to the optimal  $\beta$  which showed a monotonic increase with  $H$ , optimal  $\gamma$  and  $\phi$  showed a reversal in the trend after a critical  $H$ . Effectiveness of surface modification on the heated wall is also established through a net power analysis.

© 2021 Elsevier Ltd. All rights reserved.

## 1. Introduction

Magnetohydrodynamic (MHD) duct flows have been an ongoing subject of investigation over years due to its relevance in engineering applications such as electromagnetic casting, metallurgical applications, generators and the cooling blankets of magnetic confinement nuclear fusion reactors etc [1,2]. The problem motivating the present study is the detrimental impact of strong magnetic field confining plasma in the reactor chamber of nuclear fusion reactors on the heat transfer efficiency of the cooling blankets fluids surrounding the reactor chamber [1,3–5]. The lower heat transfer efficiency has a direct effect on the power generation efficiency of these reactors [4,6]. Electrically conducting fluids flowing under the presence of a magnetic field are subjected to a Lorentz force, produced due to the interaction of the induced current with the magnetic field. This force has a damping effect on the turbulent fluctuations, thereby laminarising the flow and diminishing convective heat transfer in such ducts [4,7,8].

Even though, the presence of a strong magnetic field results in the suppression of isotropic turbulence by Joule dissipation [9],

anisotropic turbulent structures are promoted by magnetic field by stretching the vortical structures in the direction of the magnetic field as they are least impacted by Joule dissipation [10,11]. For a conducting fluid flowing in an electrically non-conducting duct, [6] used grids in rectangular channels and observed a fall and a minimum in Nusselt number ( $Nu$ ) with increasing magnetic field strength. They associated the behaviour to the competition between isotropic and anisotropic turbulence. They also report a further rise in  $Nu$ , with increasing anisotropic vortical structures. In a subsequent study, [12] showed, the grids with axis aligned with the field direction to be favourable, as they favour the formation of vortical structures aligned with the magnetic field direction which are in the flow for longer time.

Under the influence of a strong magnetic field, velocity variations in the field directions are suppressed and are limited to the thin layers formed on the walls perpendicular to the magnetic field direction called the Hartmann layer and the flow can be described by a quasi-two-dimensional model (Q2D) [10,11]. SM82 is a Q2D model developed by [10], in which the flow variables are averaged in the magnetic field direction and a modified momentum equation obtained with an additional forcing term to account for the effect of Hartmann layer on the flow. Validity of SM82 holds under conditions when Hartmann number  $Ha \gg 1$  and interaction parameter  $N \gg 1$ . Under these conditions the time scale of momentum diffusion in the magnetic field direction is smaller

\* Corresponding author.

E-mail addresses: [sneha.murali@monash.edu](mailto:sneha.murali@monash.edu) (S. Murali), [w.alsaadi@ack.edu.kw](mailto:w.alsaadi@ack.edu.kw) (W.K. Hussam), [greg.sheard@monash.edu](mailto:greg.sheard@monash.edu) (G.J. Sheard).

**Nomenclature**

$a$	duct width (out-of-plane)
$B$	uniform magnetic field strength
$L$	half duct height
$h_w$	height of the wedge
$PR$	pressure ratio
$HR$	heat transfer ratio
$AR$	aspect ratio of the duct
$f$	friction factor
$f_0$	friction factor for a plane duct without wedges
$l_d$	total length of the duct
$l_p$	distance between consecutive wedges
$l_w$	wedge length in streamwise direction
$T_h$	hot wall temperature
$T_c$	cold wall temperature
$T_f$	bulk fluid temperature
$T$	scalar temperature field
$Re$	Reynolds number
$Re_m$	magnetic Reynolds number
$Pr$	Prandtl number
$Pe$	Peclet number
$Ha$	Hartmann number
$H$	Hartmann friction term
$N$	interaction parameter
$Nu_x$	local Nusselt number
$Nu$	time and domain averaged Nusselts number
$\bar{Nu}$	domain averaged Nusselts number
$Nu_0$	Nu for a plane duct without wedges
$Ec$	Eckert number
$P_{heat}$	heat power
$P_{0,heat}$	heat power for a plane duct
$P_{flow}$	pumping power
$P_{0,flow}$	pumping power for a plane duct
$C_p$	specific heat capacity of the fluid
$\mathbf{u}$	quasi 2D velocity vector
$U_0$	mean velocity through the duct
$p$	kinematic pressure
$t$	time
$x$	Cartesian coordinate (streamwise direction)
$y$	Cartesian coordinate (transverse direction)
$z$	Cartesian coordinate (out-of-plane direction)
<b>Greek symbols</b>	
$\beta$	blockage
$\gamma$	pitch
$\phi$	wedge angle
$\eta$	heat transfer efficiency
$\alpha$	fluid thermal diffusivity
$\nu$	fluid kinematic viscosity
$t$	time
$\rho$	fluid density
$\sigma$	magnetic permeability of the fluid
$\omega_z$	z-vorticity
$\Delta T$	temperature difference between hot and cold wall
$\delta T$	difference between the bulk fluid and hot wall temperature
$\Delta P_{net}$	net power into the duct
$\omega_{zp}$	vortex intensity of a vortex at streamwise position, $x$
$\omega_p$	vortex intensity of vortex formed at wedge tip
$\omega_{zx}$	z-vorticity at streamwise location $x$

than any other time scales in the flow. This model also assumes the Hartmann layer to remain laminar and stable.

Experiments by Frank et al. [13], Klein and Poth erat [14], showed the existence of Q2D flows at high Hartmann numbers and to persist at higher Reynolds numbers. Transition to quasi-two-dimensionality are also reported in the 3D simulations of the wake of bluff body flows at high  $Ha$  [15,16]. Sufficient agreement with SM82 was also found by Kanaris et al. [16] for  $N > 16$  at high  $Re$  for cylinder wakes. Vortex decay models using Q2D assumptions developed in [17] matched well with 3D simulations at high  $Ha$ . The model also captures the stability properties with about 10% deviation from 3D simulations [18–20]. The optimal growth magnitude and scalings using SM82 were shown to match quite well with 3D simulations for a duct flow [21] at high magnetic field strengths. Though there was existence of three-dimensionality, at high  $Ha$ , SM82 predicts the average topology reasonably well.

Different vortex generation techniques as a means to promote heat transfer have been reported in the literature for the flow of a conducting fluid through a duct. Most of the studies use the idea of promoting anisotropic vortical structures in the flow domain to promote heat transfer. Numerical studies using inhomogeneous wall conductance were studied by [22]. There are numerous heat transfer studies employing SM82 for flow simulations. [23,24] used cylindrical bluff body for vortex generation in a duct and studied the effect of varying the cylinder position and blockage on the heat transfer behaviour. They found an optimal position of the cylinder to be favourable for achieving maximum heat transfer efficiency. Flow regimes and the heat transfer enhancement with square cylinders were investigated in [25]. Similarly, [26] investigated rectangular cylinders at different angles of attack and show their optimal values with a maximum efficiency of 1.7. Further studies were conducted on active vortex promotion strategies such as, transverse [27,28] and torsional oscillation of a cylinder [29]. These studies found that a higher amplitude of oscillation of the cylinder benefitted heat transfer enhancement relative to a stationary cylinder with the existence of an optimal frequency for individual forcing amplitude [29]. Hamid et al. [30, 31], explored the use of a point electrode in the flow for vortex generation. Their study focused on the optimal positioning of the electrode in the flow and investigated the influence of various control parameters on the heat transfer efficiency.

Use of surface modification of the heated wall as means of vortex generation and heat transfer promotion in MHD duct flows have not been explored in the literature. This method has been found to be effective in heat transfer promotion in various hydrodynamic flows [32,33]. In the present study we choose a wedge-shaped wall protrusion, as this geometry showed a better heat transfer performance in hydrodynamic flow experiments [34]. Additionally, previous studies in MHD duct flows have mostly concentrated on a single vortex generator in the flow and its influence on the heat transfer behaviour. Subsequent positioning of the vortex promoters are significant, as the vortices generated are dissipated when convection downstream in the flow and the rate of dissipation increases drastically with stronger magnetic fields [17].

The present study addresses these unexplored areas by:

1. Studying the use of repeated wedge-shaped flow-facing protrusion for promoting turbulent heat transfer by anisotropic vortex generation in a Q2D MHD duct flow.
2. Quantifying the influence of a few identified geometric parameters of the protrusion and flow parameters on the heat transfer behaviour.
3. Investigating the overall efficiency of this technique for heat transfer improvement.

The paper is presented as follows: First, the problem setup, including the governing equations and parameters are presented in Section 2 followed by the numerical method used and the grid resolution study in Section 3. In the result Section 4, initially, vortex

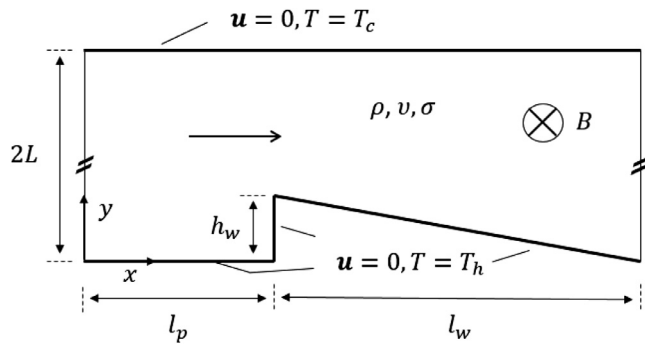


Fig. 1. Flow setup with geometric parameters and boundary conditions. Flow is left to right.

evolution in the duct and its influence on local heat transfer behaviour is elucidated as a general example, followed by detail discussion on the influence of each of the identified geometric parameter and flow parameters on heat transfer enhancement. Efficiency of the usage of wedges are described in Section 4.3. The result section is concluded by a brief comparison with other enhancement techniques, with conclusions drawn in Section 5.

## 2. Problem setup

The problem setup for the present study is shown in Fig. 1. An electrically conducting and incompressible fluid with density  $\rho$ , kinematic viscosity  $\nu$  and electrical conductivity  $\sigma$  flowing through a duct with height  $2L$  and an out-of-plane width  $a$  with a uniform magnetic field  $B$  acting along  $a$  is considered. Magnetic Reynolds number  $Re_m \ll 1$  is considered, hence the induced magnetic field is neglected. No-slip boundary condition on the bottom and top walls with a periodic streamwise ( $x$ ) condition is applied. The duct walls are electrically non-conducting where the bottom wall is maintained at a constant temperature  $T_h$ , while the top wall is maintained at a constant temperature  $T_c$ .

The following dimensionless geometric parameters are associated with the flow setup: blockage  $\beta$ , which is the ratio of the wedge height  $h_w$  to that of the duct height  $2L$ , pitch  $\gamma$ , which is the ratio of the distance between the wedges  $l_p$  to half-duct height  $L$  and wedge angle  $\phi$ , which is the angle that the tapered wedge surface makes with the horizontal, where  $\tan(\phi) = h_w/l_w$ . The geometric parameter values investigated in this study are: (i)  $\beta = 0.125, 0.25, 0.35, 0.5, 0.65$ , (ii)  $\gamma = 0.5, 1, 1.5, 2, 2.5, 3, 4, 5, 6, 8$  and (iii)  $\phi = 14.036, 9.4626, 7.125, 5.71059, 4.7636, 3.5763$ .

### 2.1. Governing equations and parameters

The flow covering the laminar and quasi-two-dimensional regimes are computed using the SM82 model, under which the dimensionless continuity, momentum and energy equation are given by:

$$\nabla \cdot \mathbf{u} = 0, \quad (1)$$

$$\frac{\partial \mathbf{u}}{\partial t} + (\mathbf{u} \cdot \nabla) \mathbf{u} = -\nabla p + \frac{1}{Re} \nabla^2 \mathbf{u} - \frac{H}{Re} \mathbf{u}, \quad (2)$$

$$\frac{\partial T}{\partial t} + (\mathbf{u} \cdot \nabla) T = \frac{1}{Pe} \nabla^2 T, \quad (3)$$

where  $\mathbf{u}$  is the quasi-two-dimensional velocity,  $p$  and  $T$  are the pressure and temperature fields respectively. Lengths are scaled by  $L$ , velocity by the mean duct velocity  $U_0$ , time  $t$  by  $L/U_0$ , pressure by  $\rho U_0^2$  and temperature by  $\Delta T = T_h - T_c$ . The viscous and Joule

heating terms in the energy equation are neglected since the order of magnitude of these terms are much lower than the thermal diffusion term. Further details on the order of magnitude analysis can be found in [35]. The present flow is considered under a forced convection condition and the effects of buoyancy has been neglected following findings from Burr et al. [36], where they found the effect of natural convection to be suppressed for flow between a hot and cold horizontal plate arrangement under a strong magnetic field strength. Similar studies such as [37,38] also support these findings and have neglected the effects of natural convection in their investigations. The non-dimensional parameters Reynolds number  $Re$ , Hartmann friction parameter  $H$  and Peclet number  $Pe$  are defined as:

$$Re = U_0 L / \nu, \quad (4)$$

$$H = n \left( \frac{L}{a} \right)^2 Ha, \quad (5)$$

$$Pe = Re Pr, \quad (6)$$

where  $n$  is the number of Hartmann walls in the duct, which for the present setup is 2,  $Ha$  is the Hartmann number defined as  $Ha = aB\sqrt{\sigma/\rho\nu}$ , square of which characterises the ratio of electromagnetic to viscous forces and  $Pr$  is the Prandtl number of the fluid defined as  $Pr = \nu/\alpha$ , where  $\alpha$  is the thermal diffusivity of the fluid.  $Pr = 0.022$  is used in this study which is representative of the eutectic lead alloy GalSn.

To verify if the flow parameters of the present study satisfies the condition of validity of the SM82 model and will have minimum discrepancy from 3D simulations, a worst case of the lowest  $H$  and highest  $Re$  considered in the study are used ( $H = 50$ ,  $Re = 2000$ ). From Eq. (5),  $Ha = 2H \times AR^2$ , where  $AR$  is the aspect ratio of the duct given by,  $a/2L$ . Considering  $AR = 1, 1.5$  &  $2$ , the corresponding  $Ha = 100, 225$  &  $400$  and  $N = 5, 25$  &  $80$  respectively, where  $N = Ha^2/Re$ . The condition for stability of the Hartmann layer found by Lingwood and Alboussiere [39] is satisfied for all the cases investigated. 3D simulations by Kanaris et al. [16] of confined flow around a cylinder have shown Q2D models to match 3D results for  $N > 16$  for high  $Re$ . For a duct with  $AR = 1$ , Q2D results might not match well with a 3D simulations for  $H = 50$ . According to results from the literature, Q2D results with  $H = 50$  in the present study with  $Re = 2000$  and  $Re = 1300$ , will match reasonably well with 3D simulations for  $AR \geq 1.33$  and  $AR \geq 1.2$  respectively. Since the  $Re$  considered is lower, quasi-two-dimensionality is expected to be satisfied for  $N < 16$ .

The overall efficiency of heat transfer is quantified by  $\eta$ , which has been used in a number of heat transfer studies [24,26,31] as a measure of efficiency.  $\eta$  is given by:

$$\eta = \frac{HR}{PR}, \quad (7)$$

where  $HR$  and  $PR$  are the heat transfer ratio, used to measure the heat transfer improvement with the presence of the wedges in the duct and the pressure ratio, which is used to measure the pressure drop penalty with the use of wedges in the duct respectively and are defined as:

$$HR = \frac{Nu}{Nu_0}, \quad (8)$$

$$PR = \frac{f}{f_0}, \quad (9)$$

where  $Nu$  and  $f$  are the domain and time averaged Nusselt number and friction factor respectively. Subscript 0 is used to denote a plane duct without wedges.  $Nu$  is defined as  $h(2L)/k$ , where  $h$

and  $k$  are respectively the convective heat transfer coefficient and thermal conductivity of the fluid.

The net circulation used to represent the intensity of a vortex at any streamwise location  $x$  is calculated as the local vorticity flux and is given by:

$$\omega_{zp} = \frac{1}{L} \int_{y_{b,x}}^{2L} \omega_{zx} dy, \quad (10)$$

where  $y_{b,x}$  is the  $y$  coordinate of the bottom wall at  $x$  and  $\omega_{zx}$  is the  $z$ -vorticity at  $x$ .

The local Nusselt number [40] along the heated bottom wall of the duct is calculated as:

$$Nu_x(x, t) = \frac{2L}{(T_{f,x} - T_h)} \frac{dT}{dn} \Big|_{y_{b,x}}, \quad (11)$$

where,  $T_{f,x}$  is the local bulk fluid temperature given by:

$$T_{f,x}(x, t) = \frac{\int_{y_{b,x}}^{2L} uT dy}{\int_{y_{b,x}}^{2L} u dy}, \quad (12)$$

where  $dT/dn_{y_{b,x}}$  is the wall normal temperature gradient at  $y_{b,x}$ . It should be noted that  $Nu_x$  does not take into account the influence of the vertical front wall of length  $l_w$  to the overall heat transfer, hence to calculate the domain average Nusselt number  $\bar{Nu}$  in the present study, we adopt the following method:

$$\bar{Nu}(t) = \frac{2L}{(T_f - T_h)} \frac{dT}{dn} \Big|_{y_b}, \quad (13)$$

where  $T_f$  is the domain averaged bulk fluid temperature calculated as:

$$T_f(t) = \frac{\int \int_{\Omega} uT d\Omega}{\int \int_{\Omega} u d\Omega}, \quad (14)$$

and  $dT/dn_{y_b}$  is the average wall normal temperature gradient from the bottom wall comprising the horizontal, vertical and the tapered surface's contribution.  $Nu$  is obtained by the time average of  $\bar{Nu}$ .

Another measure to quantify the effectiveness of the wedge in the duct is to carry out a net power balance. Similar analysis have been conducted in other studies [26,30] which used different vortex generation techniques to enhance heat transfer to the fluid. The net power to the system (duct with wedge) is calculated as:

$$\Delta P_{net} = \Delta P_{heat} - \Delta P_{flow}, \quad (15)$$

where,  $\Delta P_{heat} = P_{heat} - P_{0,heat}$  and  $\Delta P_{flow} = P_{flow} - P_{0,flow}$  are the increment in heat power and pumping power, achieved by presence of wedge in the duct.  $P_{heat}$  is the non-dimensional power gained as heat from the hot bottom wall with the wedge present in the duct whereas  $P_{flow}$  is the non-dimensional power spent on pumping the fluid through the flow domain comprising the wedges. Subscript 0 is used to denote the corresponding power for a plane duct without wedges.  $P_{heat}$  is expressed as:

$$P_{heat} = \frac{\alpha C_p}{L^2 U_0^3} \int_0^{l_d} \frac{dT}{dn} dx, \quad (16)$$

where  $C_p$  is the specific heat capacity of the fluid and  $l_d = l_p + l_w$  is the total length of the duct. Eq. (16) can be re-written in terms of  $Nu$  as:

$$P_{heat} = \frac{\alpha C_p l_d \delta T}{L^3 U_0^3} Nu, \quad (17)$$

where,  $\delta T = T_h - T_f$ .  $P_{flow}$  is expressed as:

$$P_{flow} = \frac{2a}{L} \Delta p \quad (18)$$

where  $\Delta p$  is the non-dimensional pressure drop in the duct. Eq. (18) can be re-written in terms of  $f$  as:

$$P_{flow} = \frac{al_d}{L^2} f. \quad (19)$$

From Eqs. (15), (17) and (19),  $\Delta P_{net}$  is given by:

$$\Delta P_{net} = \frac{\alpha C_p l_d \delta T}{L^3 U_0^3} (Nu - Nu_0) - \frac{al_d}{L^2} (f - f_0). \quad (20)$$

Multiplying by  $L^2/al_d$ ,  $\Delta P_{net}$  can be simplified as:

$$\Delta P_{net} = \frac{1}{PeEc} (Nu - Nu_0) - (f - f_0), \quad (21)$$

where,  $Ec$  is the Eckert number, defined as  $U_0^2/C_p \delta T$ . It is a measure of the kinetic energy at the wall to the specific enthalpy difference between the hot wall and the fluid.

### 3. Numerical method and grid resolution

The simulations reported herein uses an in-house solver, based on a nodal spectral element method for spatial discretisation of the governing equations and a third order backward multistep method for time integration [41]. In this method, Lagrangian tensor product polynomial basis function are used within each element and interpolation carried out at Gauss-Legendre-Lobatto (GLL) quadrature points. This discretisation technique allows for a two-way refinement in terms of the number of elements (h-refinement) and polynomial order (p-refinement) [42]. An exponential convergence is possible with increasing polynomial orders. The solver has been validated for numerous hydrodynamic and quasi-two-dimensional flow simulations [17,21,43,44] and heat transfer problems [24,26,31]. To further validate the  $Nu$  calculated, a comparison of the analytical Nusselt number for a plane duct without wedges  $Nu_0$  under a purely conductive heat transfer condition is made with the  $Nu^*$  obtained by numerical simulation for the same case. The relative error for  $Nu^*$  computed from the simulation was found to be less 0.0001% from analytical solution  $Nu_0$  obtained for the purely conduction dominated case.

Grid independence testing was conducted at two  $H$  values and a high  $Re$  and are reported in Table 1. The time averaged  $\mathcal{L}^2$  norm,  $f$  and  $Nu$  are used as testing parameters for a case with geometric setting of  $\beta = 0.25$ ,  $\gamma = 2$  and  $\phi = 7.125$ . The mesh for the tested setup consists of 594 elements with grading towards the walls. They were tested for polynomial orders ranging from  $n_p = 8$  to 18. Based on convergence of the tested parameter,  $n_p = 15$  was selected for the simulations with this geometric parameter setting, which gave a maximum of 0.5% relative error with respect to  $n_p = 18$  for the worst case. For other  $\beta$ ,  $\gamma$  and  $\phi$  simulated in the current study, the number of elements used and their grading towards the wall were decided such that the size of the smallest and largest element were similar to the tested case. The same polyno-

**Table 1**

Grid resolution for different order of polynomial ( $n_p$ ) for geometric setting  $\beta = 0.25$ ,  $\gamma = 2$  and  $\phi = 7.125$ . Quantities shown are the time averaged  $\mathcal{L}^2$  norm, friction factor ( $f$ ) and Nusselt number  $Nu$  for  $H = 500$ , 5000 at  $Re = 3000$ .

$H = 500$ and $Re = 3000$			
$n_p$	$\mathcal{L}^2$ norm	$f$	$Nu$
8	15.24208351	0.439860135	2.81698945
10	15.25299113	0.44061984	2.83743227
12	15.27576248	0.44151360	2.82205526
15	15.27470995	0.44086007	2.84591718
18	15.33838270	0.44234412	2.82845062
$H = 5000$ and $Re = 3000$			
$n_p$	$\mathcal{L}^2$ norm	$f$	$Nu$
8	13.79156379	3.86286491	2.24203982
10	13.79052610	3.86220163	2.24185988
12	13.78995431	3.86176570	2.24223117
15	13.79285921	3.85823891	2.24060611
18	13.78752563	3.84658545	2.23422859

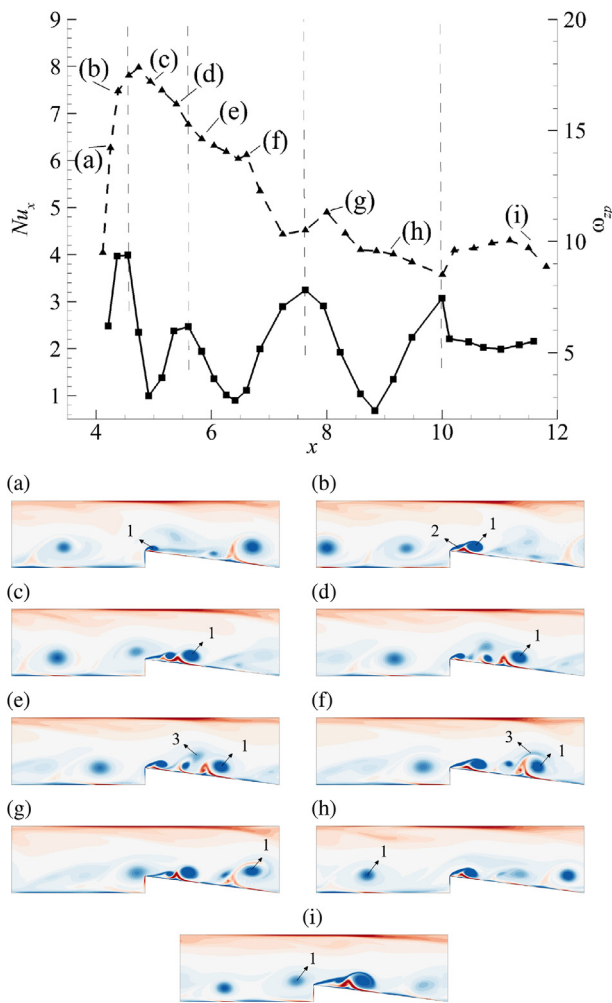


**Fig. 2.** Plot showing the evolution of vortex strength ( $\omega_{zp}$ ,  $\blacktriangle$ ; dashed line for guidance) and local instantaneous Nusselt number ( $Nu_x(x, t)$ ,  $\blacksquare$ ; solid line for guidance) plotted against streamwise position  $x$ . Values of  $\omega_{zp}$  are obtained from the trajectory of vortex labelled “1” in the accompanying sequence of vorticity contour plots (a)–(i). This case has  $\beta = 0.25$ ,  $\gamma = 4$ ,  $\phi = 7.125$ ,  $Re = 1300$  and  $H = 50$ . 20 equispaced vorticity contour levels are plotted between  $-10$  (blue) and  $10$  (red). (For interpretation of the references to color in this figure legend, the reader is referred to the web version of this article.)

mial order of 15 was used for all subsequent simulations reported herein.

**4. Results and discussions**

**4.1. Flow field - vortex evolution and influence on local Nusselt number**

In this section, the evolution of a vortex in the flow domain in terms of variation of its vortex intensity ( $\omega_{zp}$ ) and its influence on the local instantaneous Nusselt number  $Nu_x(x, t)$  are elucidated for a case with  $Re = 1300$ ,  $H = 50$ ,  $\beta = 0.25$ ,  $\gamma = 4$  and  $\phi = 7.125$  (Fig. 2). The intensity of the vortex at location  $x$  is calculated as given in Eq. (10). The peak  $Nu_x$  lags slightly behind the peak vortex intensity. The presence of the wedge results in vortex formation (represented as 1) starting at the wedge tip as shown in Fig. 2(a). This vortex extends downstream remaining attached to the wedge tip, while a second smaller vortex (represented as 2) starts forming behind it (Fig. 2(b)). The strength of the vortex increases with  $x$  when attached to the tip.  $Nu_x$ , achieves a peak during vortex formation. With the formation of 2 behind 1, shown

in Fig. 2(b),  $Nu_x$  drops. With the growth of 2, the larger vortex 1 deattaches itself from the wedge tip, which is associated with a drop in its strength (Fig. 2(c)). Similar behaviour of a second vortex formation and detachment of the primary vortex was also observed in [17], where a point electrode was used as vortex generator. Vortex 1, then convects downstream along the wedge taper with its strength decaying during its evolution as can be seen from Fig. 2(d-f). An increase in  $Nu_x$ , during its convection downstream is associated with the interaction of the convecting vortex with the wall vortices. On interaction and merging with a vortex convecting from upstream represented as 3 (refer Fig. 2(d,e)), vortex 1 gains strength, which is observed as a jump in the intensity curve. The rise in intensity on vortex merging depends on the intensity of the two merging vortices. A subsequent rise in  $Nu_x$  can be observed, illustrating the favourable effect of vortex merging on  $Nu$ . Vortex 1, then convects into the gap between the wedges with decaying intensity (Fig. 2(g,h)). On approaching the wedge, vortex 1 accelerates over the wedge, sweeping with it the secondary wall vortices, which explains the increasing  $Nu_x$  in that region (Fig. 2(i)). Thereafter, vortex 1 interacts with the new vortex forming at the next wedge tip. The interplay of vortex formation at the wedge tip, its intensity, interaction of the convecting vortices with the wall vortices and interaction and merging with the incoming vortices play a key role in the heat transfer behaviour of the system. The convecting vortices and its interactions are influenced by the flow conditions and geometric parameter setting of the wedge. In the subsequent sections, the heat transfer behaviour and its dependence on each of these influencing parameters are discussed in detail.

**4.2. Heat transfer ratio HR**

In this section, the heat transfer ratio ( $HR$ ) achieved by the use of wedges and its dependence on blockage  $\beta$ , pitch  $\gamma$ , wedge angle  $\phi$ , Hartmann friction  $H$  and  $Re$ , the associated flow structures and its effect on heat transfer rate from the heated wall are presented. The effect of geometric parameter variations of the wedge for a case with  $Re = 1300$  for  $H = 50$  and the influence of a range of  $H$  from  $H = 0$  (hydrodynamic case) to  $H = 500$  are discussed. For a higher  $H$  of 500, the effect of  $Re = 1500$  to 3000 are also presented.

**4.2.1. Effect of blockage  $\beta$**

$HR$  variation with blockage is shown in Fig. 3 for  $Re = 1300$  and  $H = 50$ . A monotonic increase in  $HR$  with  $\beta$  is observed.  $HR$  increases at a lower rate with  $\beta$  until approximately  $\beta = 0.3$ , after

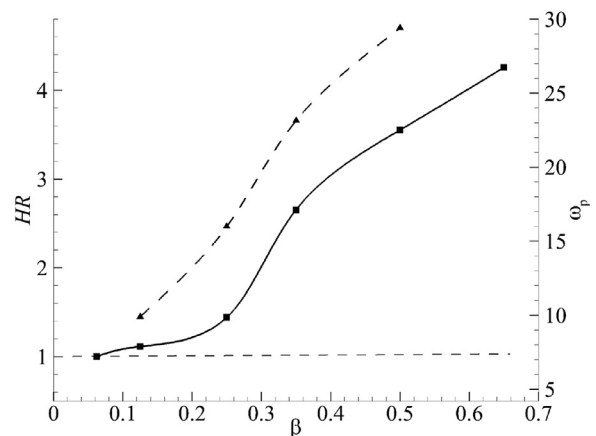


**Fig. 3.** Variation of  $HR$  ( $\blacksquare$ ; solid spline for guidance) and the intensity of the vortex formed at the wedge tip before deattachment ( $\blacktriangle$ ; dashed spline for guidance) with  $\beta$  for  $Re = 1300$ ,  $H = 50$  and  $\beta = 0.25$ . Dashed horizontal line represents  $HR$  for a duct with no wedges.

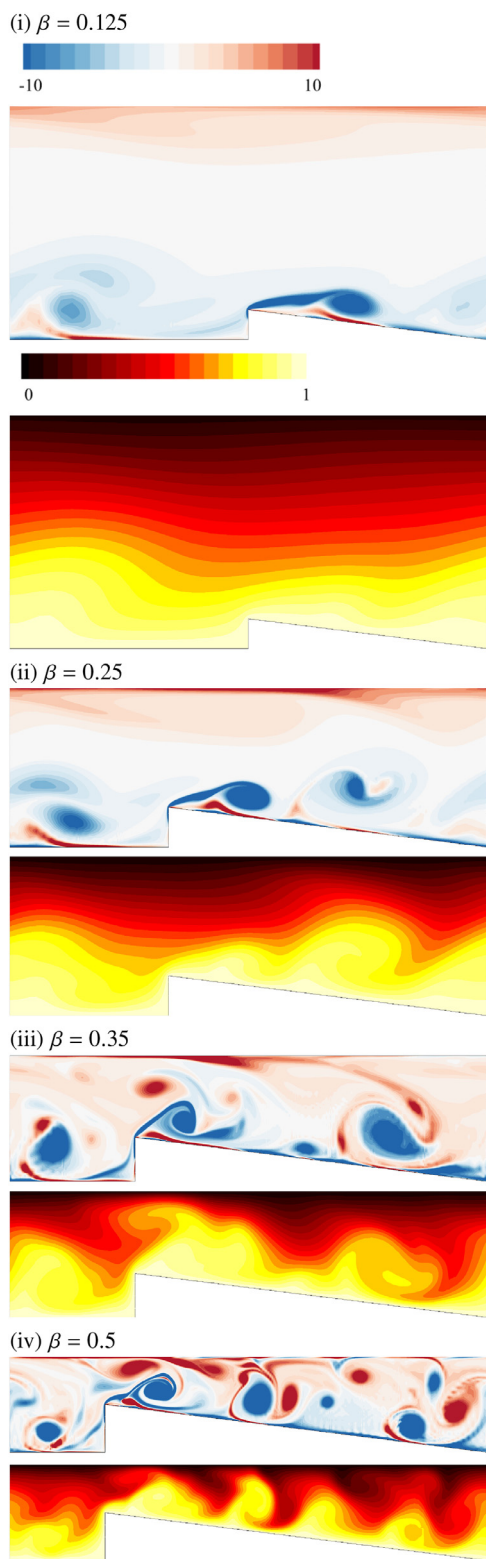


**Fig. 4.** Contours of spanwise vorticity ( $\omega_2$ ) (above) and temperature field (below) for (i)  $\beta = 0.125$ , (ii)  $\beta = 0.25$  (iii)  $\beta = 0.35$  and (iv)  $\beta = 0.5$  for  $Re = 1300$  and  $H = 50$ . 20 contour levels between  $-10 \leq \omega_2 \leq 10$  are displayed for the vorticity contours. Temperature contours are shown in the range  $T_h \leq T \leq T_c$  with the dark and light contour levels representing the cold and hot fluid respectively.

which it increases at a relatively higher rate with  $\beta$ . An instantaneous snapshot of the flow field and the temperature field for  $\beta = 0.125, 0.25, 0.35$  and  $0.5$  are shown in Fig. 4. It can be observed that the size of the vortex formed at the wedge tip scales

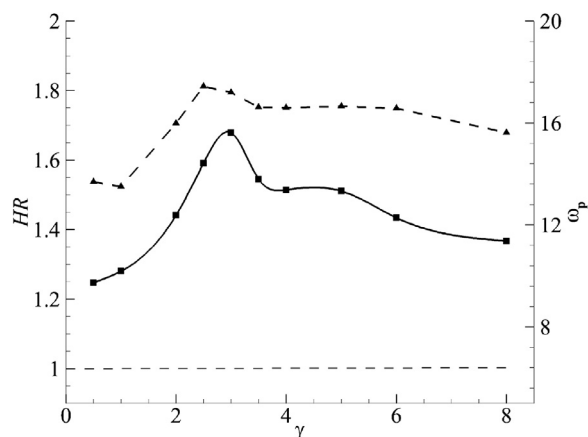


**Fig. 5.** Variation of  $HR$  (■; solid spline for guidance) and the intensity of the vortex formed at the wedge tip before deattachment (▲; dashed spline for guidance) with  $\gamma$  for  $Re = 1300$ ,  $H = 50$  and  $\beta = 0.25$ . Dashed horizontal line represents  $HR$  for a duct with no wedges.

roughly with the height of the wedge. With increasing  $\beta$ , the vortices formed at the wedge tip are more intense. The intensity of the vortex formed at the wedge tip before it dettaches from the wedge tip are shown in Fig. 3 for different blockages. These vortices formed at the wedge tip rolls up and are cast away from the tapered wall with increasing  $\beta$ , before deattaching itself from the tip and convecting downstream. The convecting vortices interact with the secondary wall vortices on the top wall of the duct in addition to those on the bottom wall at higher blockage, resulting in better mixing of the hot fluid near the bottom wall and the cold fluid near the top wall of the duct. This is evident from the temperature field where more dominant plume structures are observed with increasing  $\beta$ . For  $\beta = 0.5$ , the convecting vortices engulfs the wall vortices on the top wall resulting in counter-rotating vortex pair forming on the wedge taper wall, disrupting the thermal-boundary layer and helping to achieve higher  $HR$ .

#### 4.2.2. Effect of pitch $\gamma$

For a fixed blockage of  $\beta = 0.25$  and  $H = 50$ ,  $HR$  achieves a peak value, at an optimal pitch  $\gamma_{opt,HR}$ , as shown in Fig. 5. An instantaneous snapshot of the corresponding flow and temperature field for  $\gamma = 1, 2, 3, 4$  and  $8$  are shown in Fig. 6. For  $\gamma = 1$ , vortex interactions occur only on the wedge taper walls, whereas with a gradual increase in  $\gamma$ , additional vortex interactions can occur in the gap between the wedges. With further increase in the pitch, the convecting vortices are less intense (Fig. 5). Due to larger convecting distance, the vortices are more damped before reaching the subsequent wedge. Weaker convecting vortices do not strongly interact with the secondary wall vortices in the gap between the wedges which decreases its impact on the thermal boundary layers leading to a lower  $Nu_x$  as explained in Section 4.1. Study by Hamid et al. [17] found that a vortex in the near wake of a quasi-two-dimensional MHD flow is subjected to a higher viscous damping near the wake. On convecting further away from the wake, hartmann damping becomes predominant over viscous damping which has a drastic impact on lowering the vortex intensity. The intensity of the vortex formed at the wedge tip increases with  $\gamma$ , until  $\gamma_{opt,HR}$  (Fig. 5).  $\gamma_{opt,HR}$  is most favourable, as it allows for multiple vortex merging of intense vortices which helps increase  $Nu_x$  and thereby  $HR$ . On increasing  $\gamma$  above  $\gamma_{opt,HR}$ , not only is the intensity of the formed vortices reduced but is subjected to a higher hartmann damping when convecting downstream, as it now has to travel a greater distance before the next wedge to gain strength. This might be the reason for reducing  $HR$  when  $\gamma > \gamma_{opt,HR}$ .

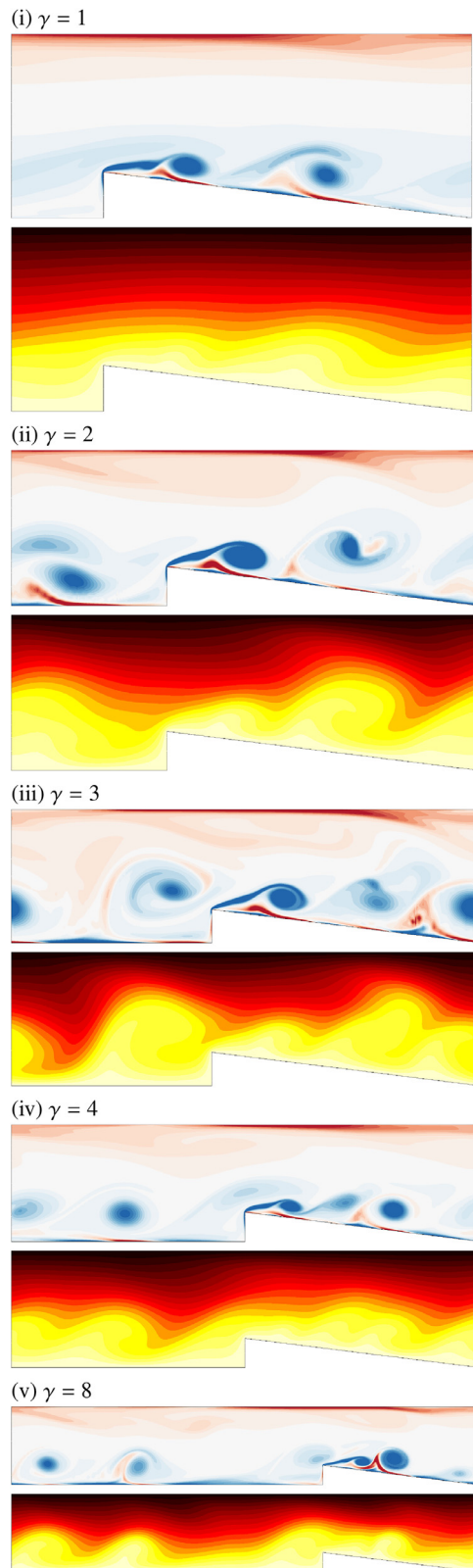


**Fig. 6.** Contours of spanwise vorticity ( $\omega_2$ ) (above) and temperature field (below) for (i)  $\gamma = 1$ , (ii)  $\gamma = 2$ , (iii)  $\gamma = 3$ , (iv)  $\gamma = 4$  and (v)  $\gamma = 8$  for  $Re = 1300$  and  $H = 50$ . The contour levels are same as in Fig. 4.

#### 4.2.3. Effect of wedge angle $\phi$

Variation of  $HR$  with wedge angle is shown in Fig. 7. Similar to  $\gamma$ , there also exists an optimal  $\phi$  at which maximum  $HR$  can be attained  $\phi_{opt,HR}$ . For a fixed  $\beta$  and  $\gamma$ , increasing  $\phi$  not only increases

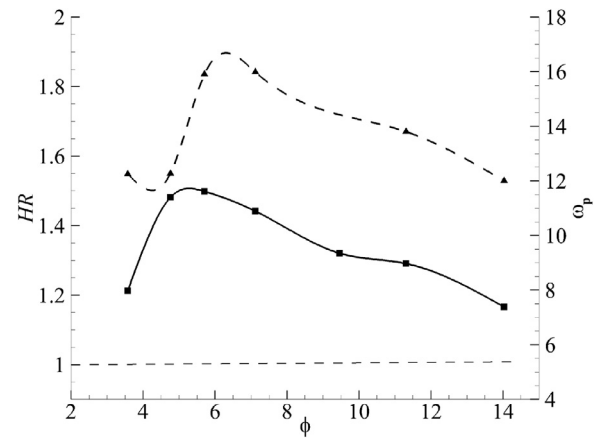


**Fig. 7.** Variation of  $HR$  (■; solid spline for guidance) and the intensity of the vortex formed at the wedge tip before deattachment (▲; dashed spline for guidance) with  $\phi$  for  $Re = 1300$  and  $H = 50$ . Dashed horizontal line represents  $HR$  for a duct with no wedges.

the inclination of the tapered surface of the wedge, but also decreases the length of the wedge or shortening the distance to the next wedge. Fig. 8 shows instantaneous flow field and temperature field for a range of wedge angles investigated. With a steeper inclination  $\phi = 14.036$  of the wedges (Fig. 8(i)), the vortices are cast away from the taper wall during its formation resulting in lesser interaction with the wall vortices. The shorter wedge length is also not favorable for interactions with convecting vortices. With decreasing  $\phi$ , until  $\phi_{opt,HR}$ , the vortices formed at the tip are cast relatively closer to the wedge walls, allowing for better interactions with the wall vortices and a wedge length allowing for interaction of convecting vortices. With further decrease beyond the optimal angle of the wedge, the vortices formed are less intense and the interacting convecting vortices are weaker, resulting in weaker interaction with wall vortices and a lower  $HR$ . The temperature contours shown in Fig. 8 (i), (ii) and (v) shows a diffusively dominated flow at smaller and larger wedge angles and the plume structures at intermediate wedge inclinations, Fig. 8 (iii and iv), increasing the convective heat transfer from the hot wall. This kind of behaviour was also observed in [24], in which existence of an optimal gap height (measure of distance of a cylinder from the hot wall) favouring maximum enhancement in  $HR$  was found. By varying gap height, the study tried to vary the way the vortices generated by the cylinder were cast on the hot wall and its interactions with the wall vortices. Decreasing gap height helped better interaction with wall vortices and after an optimal distance, further movement closer to the wall suppressed the vortices due to interaction with Shercliff layers.

#### 4.2.4. Effect of hartmann friction ( $H$ )

The influence of Hartmann friction ( $H$ ) on  $HR$  is depicted in Fig. 9, where  $H = 0$  is the corresponding two-dimensional hydrodynamic case. A monotonic decrease in  $HR$  which asymptotes to a constant value with  $H$  is observed for all  $\beta$ . It can be seen from Fig. 9 that increasing the blockage  $\beta$  has a positive effect on  $HR$ . A broader range of  $H$ , with  $HR > 1$  can be achieved by increasing the blockage. A higher blockage also asymptotes to a larger  $HR$  at high  $H$  as indicated in the figure. Increasing  $H$  has a detrimental effect on  $HR$ , as it plays the role of dissipating the energy of the quasi-2D vortices generated by the protrusion on the wall. The reduction in vortex intensity lowers the impact on the  $Nu_x$ , thereby reducing  $HR$ . For a given  $\beta$  and  $H$ , there exists an optimal pitch  $\gamma$  and optimal wedge angle ( $\phi$ ), corresponding to the highest  $HR$  that can be achieved (Fig. 10). With increasing  $H$ , both  $\gamma_{opt,HR}$  and  $\phi_{opt,HR}$ ,

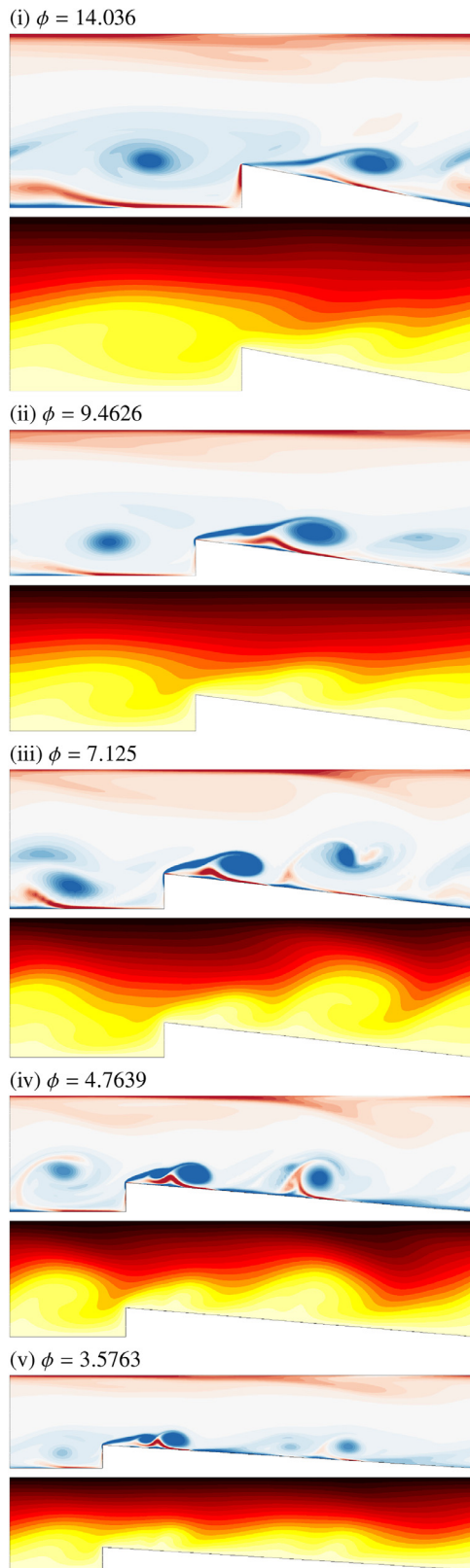


**Fig. 8.** Contours of spanwise vorticity ( $\omega_z$ ) (above) and temperature field (below) for (i)  $\phi = 14.036$ , (ii)  $\phi = 9.4626$ , (iii)  $\phi = 7.125$ , (iv)  $\phi = 4.7639$  and (v)  $\phi = 3.5763$  for  $Re = 1300$  and  $H = 50$ . The contour levels are same as in Fig. 4

first increases and then decreases. For the highest  $H$  investigated in this study, consecutive wedges with no gap between them is most favourable to achieve maximum  $HR$ .

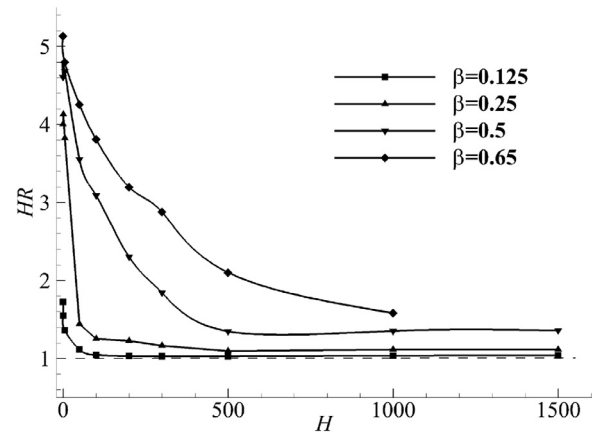


**Fig. 9.** Variation of  $HR$  with  $H$  for  $Re = 1300$  for different  $\beta$  as indicated. Dashed horizontal line represents  $HR$  for a duct with no wedges.

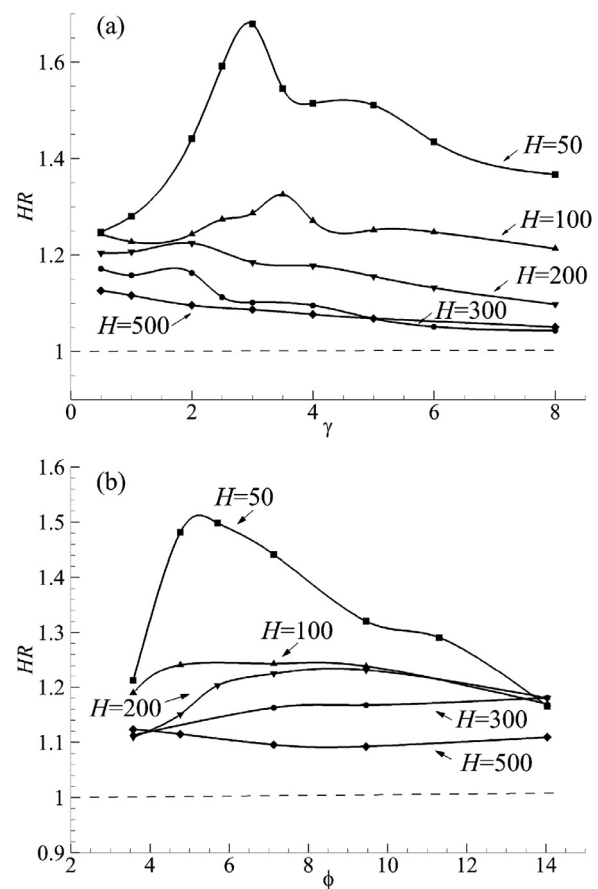


**Fig. 10.** Variation of  $HR$  for  $\beta = 0.25$  for  $Re = 1300$  with (a)  $\gamma$  and (b)  $\phi$  for 50, 100, 200, 300 and 500.

4.2.5. Dependence on Reynolds number ( $Re$ )

The variation of  $HR$  with  $Re$  is shown in Fig. 11 for  $H = 500$ . In the steady state,  $HR$  remains almost constant with increasing  $Re$  and a higher  $HR$  is associated with the highest  $\beta$ . With the onset of vortex shedding, the flow becomes unsteady and  $HR$  increases approximately linearly with  $Re$ . Similar to the steady state, a higher blockage is favourable to achieve higher  $HR$  in the unsteady state as well. In addition to preponing the onset of vortex shedding to lower  $Re$ , the rate of  $HR$  rise with  $Re$  is also higher at higher  $\beta$ . Similar to its dependence on  $H$ , for a fixed blockage an optimal  $\gamma$  and  $\phi$  exists for different  $Re$  (Fig. 12). At  $Re = 1500$ , the flow re-

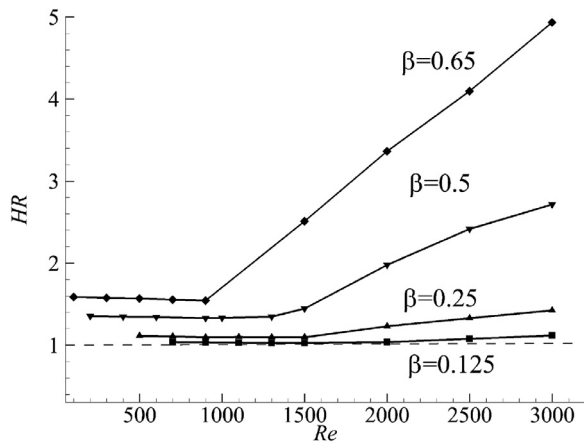


Fig. 11. Variation of HR with  $Re$  for  $H = 50$  for different  $\beta$  as indicated. Dashed horizontal line represents HR for a duct with no wedges.

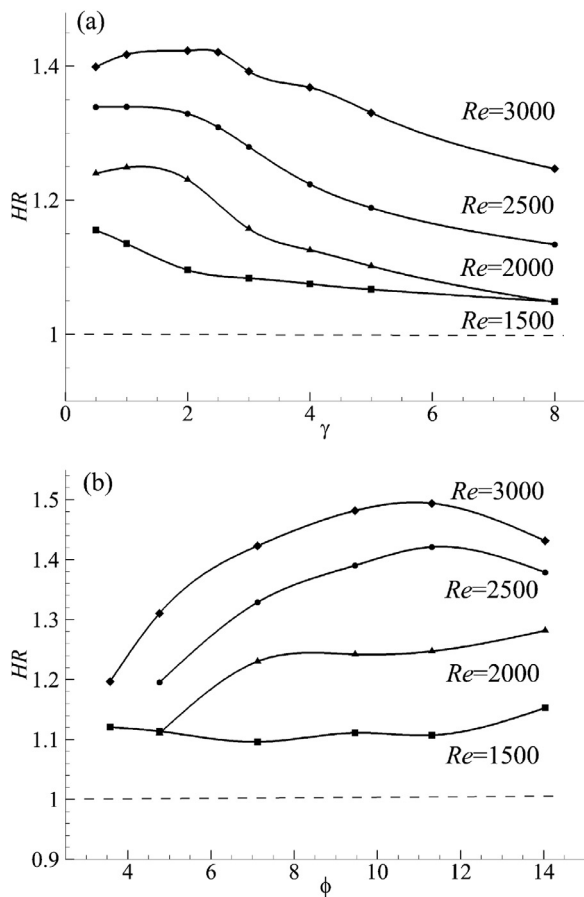


Fig. 12. Variation of HR for  $\beta = 0.25$ ,  $H = 50$  with (a)  $\gamma$  and (b)  $\phi$  for  $Re = 1500$ , 2000, 2500 and 3000.

mains in the steady state for  $\gamma \gtrsim 2$ . Decreasing  $\gamma$  further, triggers unsteadiness, causing HR to rise for  $\gamma < 2$ . In this case, consecutive wedges with no gap between them is most favourable for heat transfer increase. With increasing  $Re$ , a shift to higher optimal  $\gamma$  is observed. The higher wedge angle gives maximum HR at  $Re = 1500$ . With increasing  $Re$ , wedge angle giving maximum HR shifts to lower values.

#### 4.3. Heat transfer efficiency $\eta$

The previous sections illustrated the effectiveness of using wedge shaped protrusions for enhancing the heat transfer rate from the heated wall to the fluid flowing through the duct and optimal geometric parameters for the flow conditions investigated. Flow through ducts are subjected to pressure losses and it is important to consider the frictional losses and associated pressure penalties with the use of the wedges. In this section, the overall efficiency of the wedges for heat transfer enhancement with respect to its pressure loss penalties are discussed. This is quantified by heat transfer efficiency  $\eta$ , as defined in Eq. (7).

Fig. 13 (a) shows the influence of blockage on  $\eta$  for  $Re = 2000$  and a range of  $H$ . A non-monotonic trend in  $\eta$  with  $\beta$  can be seen for  $H = 50$  to 300. For every  $H$ , an optimal  $\beta$ ,  $\beta_{opt,\eta}$  exists corresponding to maximum  $\eta$  which shifts to a higher value with  $H$ .  $\eta < 1$  corresponds to cases which are not effective for heat transfer enhancement as the pressure drop dominates the heat transfer improvement achieved. Maximum  $\eta$  is achieved when the separation between HR and PR is maximum. This is illustrated in Fig. 14 for  $H = 200$ . For a fixed blockage,  $\gamma$  and  $\phi$  can be set to attain the best performance in terms of maximising  $\eta$ . The corresponding values are denoted as  $\gamma_{opt,\eta}$  and  $\phi_{opt,\eta}$  respectively. Fig. 13(b) and (c) shows the variation of  $\eta$  with  $\gamma$  and  $\phi$  for a range of  $H$ . Both  $\gamma_{opt,\eta}$  and  $\phi_{opt,\eta}$  show a non-monotonic trend with  $H$ . A reversal in trend in the optimal values is observed between  $H = 200$  and 300. This corresponds to a critical  $H$ ,  $H_{cr}$ , where the maximum  $\eta$  is attained for a given parameter setting. Existence of  $H_{cr}$  is observed only beyond a range of  $\beta$ ,  $\gamma$  and  $\phi$ , upto which  $\eta$  drops unvaryingly with  $H$ .

#### 4.4. Net power analysis

Similar to  $\eta$ , another useful quantity to measure the effectiveness of protrusions is the net power gained or lost by the system [26,30]. For the current setup  $\Delta P_{net}$  was calculated for a range of  $Ec$  as discussed in Section 2.1.  $Ec_{cr}$  gives the critical  $Ec$  where  $\Delta P_{net}$  changes from positive to negative, representing power gain and loss by the system respectively. Fig. 15 shows  $Ec_{cr}$  as a function of  $H$  for  $Re = 1300$  for two representative blockages,  $\beta = 0.25$  and 0.65. For fusion relevant conditions  $Ec$  ranges from about  $4.787 \times 10^{-09}$  to  $4.838 \times 10^{-09}$ , obtained using quantities relevant for fusion condition as given in [45] and properties of fluids as given in [46,47]. The lowest  $Ec_{cr}$  for the current setup is around  $2.928 \times 10^{-02}$  indicating that there is always a net positive power gain for the current setup not just for fusion relevant conditions but also for a large range of  $Ec$  below  $Ec_{cr}$ .

#### 4.5. Comparison with other enhancement techniques

In this section, a comparison of the performance of the present setup for heat transfer enhancement in quasi-two-dimensional MHD duct flows is made with other techniques which are available in the literature. While the efficiency of other wall protrusion strategies is not reported in the literature, the performance of the current approach can be compared against methods incorporating either immersed physical obstacles or electrically driven vortices. In a previous study considering the use of a bluff body for vortex generation [24], with a parameter setting of  $H = 100$  and  $Re = 2000$ ,  $\eta$  of approximately 2.2 was obtained for the best case. The current setup achieves  $\eta$  of approximately 1.5 for the highest  $\beta$ . A further increase can be achieved by setting it up at optimal  $\gamma$  and  $\phi$ . The previous study did not consider cases with higher  $H$ , where there is a possibility of drastic reduction in  $\eta$ . The present setup is effective even at higher  $H$  (refer Section 4.3). The current setup also seems to be more favourable for cases with

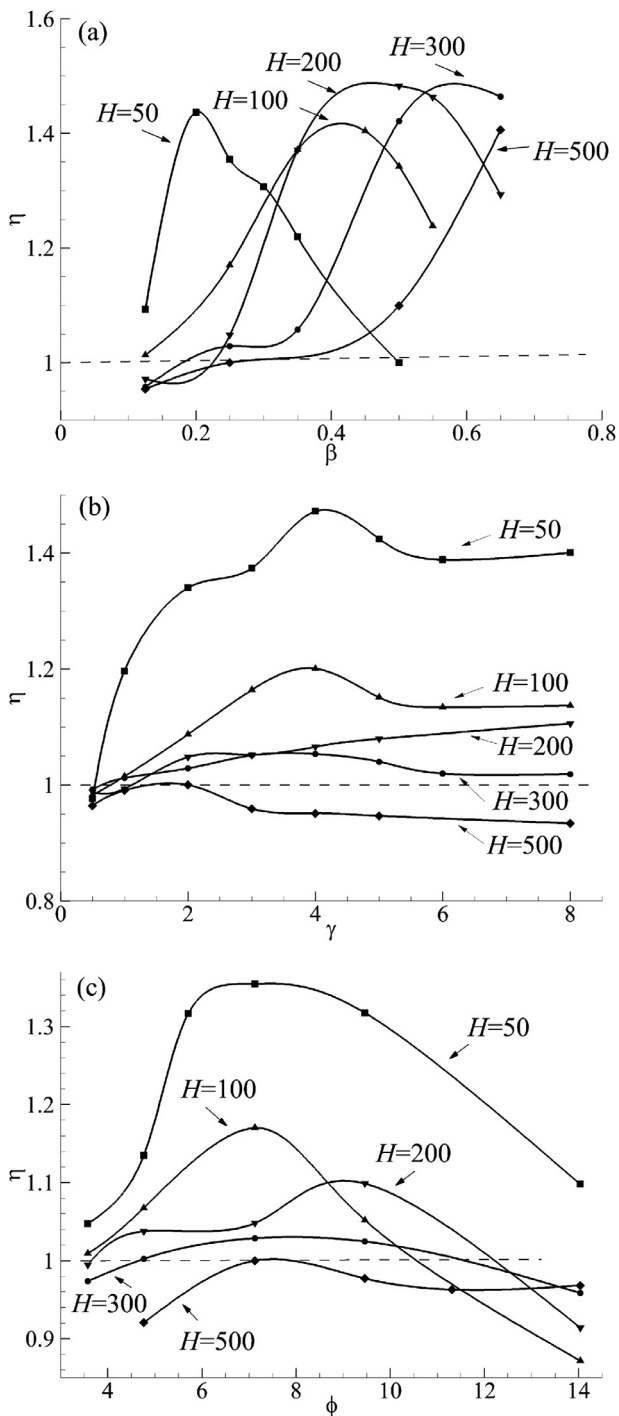


Fig. 13. Variation of  $\eta$  for  $Re = 2000$  with (a)  $\beta$  (b)  $\gamma$  and (c)  $\phi$  for  $H = 50, 100, 200, 300$  and  $500$ .

lower  $H/Re$  compared to using point electrodes for vortex generation [30], which achieves relatively higher  $\eta$  for higher  $H/Re$ . For similar flow parameters as in [29], where a torsionally oscillating cylinder was used as turbulent generator, the current setup can reach much higher  $Nu$  ( $\approx 6.39$ ) than the best case reported in the study which was about 2.6. Additionally, designing the current setup needs only a modification on the wall and no additional power requirement and mounting arrangements which may be required for previous setups.

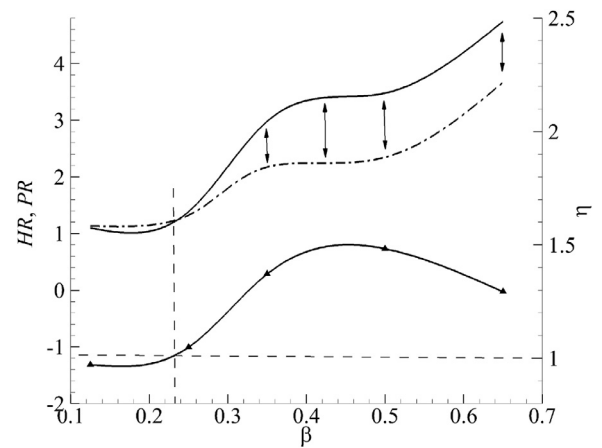


Fig. 14. Variation of  $HR, PR$  and  $\eta$  for  $\beta = 0.25, Re = 2000$  and  $H = 200$ , shown as solid, dash-dotted and solid line with symbols respectively. To the left of the dashed vertical line  $PR$  dominates over  $HR$  whereas on its right,  $HR$  takes over  $PR$ . Maximum area between the  $HR$  and  $PR$  curve corresponds to the maximum in  $\eta$ .

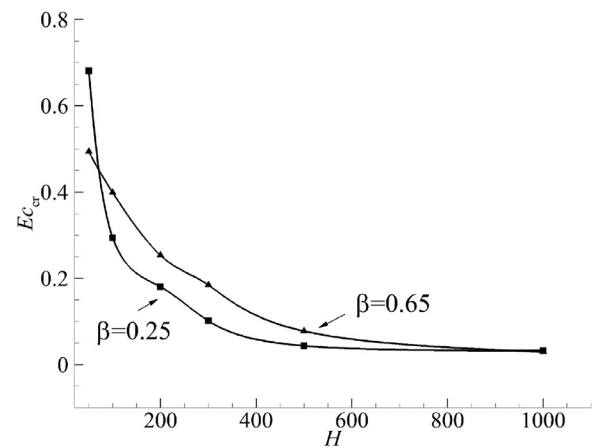


Fig. 15.  $Ec_{cr}$  as a function of  $H$  for  $Re = 1300$  for  $\beta = 0.25$  and  $0.65$ .

### 5. Conclusions

In the present study, repeated flow-facing wedge-shaped protrusions on the hot wall of a duct were investigated as a means to promote heat transfer in a Q2D MHD flow. Numerical simulations using Spectral element method were conducted for a range of Hartmann friction parameters  $50 \leq H \leq 500$ , and Reynolds number  $1300 \leq Re \leq 3000$ . Systematic variation of geometric parameters, blockage  $0.125 \leq \beta \leq 0.65$ , pitch  $0.5 \leq \gamma \leq 8$  and wedge angle  $3.576 \leq \phi \leq 14.036$  were considered. Vortex evolution, its intensity variation from its generation at the wedge tip to convecting over to the subsequent wedge and influence on local Nusselt number was discussed.  $Nu_x$  peaked just behind locations where the forming or the convecting vortex interacted with the boundary layer. Vortex merging and the presence of the subsequent wedge were favorable for maximising these interactions and thereby  $Nu_x$ .

The influence of  $\beta, \gamma, \phi$  on heat transfer ratio  $HR$ , were discussed for  $Re = 1300$  and  $H = 50$ . A monotonic rise in  $HR$  was obtained with  $\beta$  in the range investigated. For a fixed  $\beta$ ,  $HR$  could be improved further and can achieve a maximum by varying  $\gamma$  and  $\phi$  to  $\gamma_{opt,HR}$  and  $\phi_{opt,HR}$  respectively. A high  $\beta$  achieves a higher  $HR$  for all  $H$ . Both  $\gamma_{opt,HR}$  and  $\phi_{opt,HR}$  showed an increase followed by a decrease in its value with increasing  $H$ . Variation of  $HR$  with  $Re$  were also considered. At all  $Re$  the highest  $\beta$  gave the highest  $HR$ .  $\gamma_{opt,HR}$  shifted to larger  $\gamma$  with  $Re$  unlike  $\phi_{opt,HR}$  which shifted to smaller  $\phi$ .

Further, the effectiveness of using wedge shaped protrusions on the side wall of the duct was established by considering two different quantitative measures - heat transfer efficiency and net power. Heat transfer efficiency considers the enhancement in heat transfer relative to the pressure drop penalty. Its variation with  $\beta$ ,  $\gamma$ ,  $\phi$  and  $H$  are discussed for  $Re = 2000$  for the same geometric parameters and  $H$  used for  $HR$ . Different  $H$  has a range of  $\beta$ ,  $\gamma$  and  $\phi$  where it can operate effectively, i.e:-  $\eta > 1$ , with an associated optimal setting to reach  $\eta_{max}$ . Certain configurations also showed an existence of a critical  $H$ . By net power analysis, effectiveness is measured in terms of the overall power gained or lost by the system. Critical Eckert number  $Ec_{cr}$  for  $\beta = 0.25$  &  $0.65$  and its variation with  $H$  were examined for  $Re = 1300$ . The current setup was found to be effective for power gain  $\Delta P_{net} > 0$  for a large range of  $Ec$ , including fusion relevant conditions. In the end, a short comparison of the efficiency for the present setup with other heat transfer enhancement techniques are made.

### Declaration of Competing Interest

We wish to confirm that there are no known conflicts of interest associated with this publication and there has been no significant financial support for this work that could have influenced its outcome.

We confirm that the manuscript has been read and approved by all named authors and that there are no other persons who satisfied the criteria for authorship but are not listed. We further confirm that the order of authors listed in the manuscript has been approved by all of us.

We confirm that we have given due consideration to the protection of intellectual property associated with this work and that there are no impediments to publication, including the timing of publication, with respect to intellectual property. In so doing we confirm that we have followed the regulations of our institutions concerning intellectual property.

We understand that the Corresponding Author is the sole contact for the Editorial process (including Editorial Manager and direct communications with the office). He is responsible for communicating with the other authors about progress, submissions of revisions and final approval of proofs. We confirm that we have provided a current, correct email address which is accessible by the Corresponding Author and which has been configured to accept email from.

### CRediT authorship contribution statement

**Sneha Murali:** Conceptualization, Formal analysis, Investigation, Visualization, Writing - original draft. **Wisam K. Hussam:** Writing - review & editing. **Gregory J. Sheard:** Conceptualization, Software, Resources, Writing - review & editing, Supervision.

### Acknowledgements

S.M. receives an Australian Government RTP and Monash International Tuition Scholarship. This research is supported by Australian Research Council Discovery Grant DP180102647, the National Computational Infrastructure, Pawsey Supercomputing Centre, and the Monash MonARCH machine.

### References

- [1] L. Barleon, V. Casal, L. Lenhart, MHD flow in liquid-metal-cooled blankets, *Fusion Eng. Des.* 14 (1991) 401–412.
- [2] U. Müller, L. Bühler, *Magnetofluidynamics in Channels and Containers*, Springer, 2013.
- [3] S. Smolentsev, R. Moreau, M. Abdou, Characterization of key magnetohydrodynamic phenomena in PbLi flows for the US DCLL blanket, *Fusion Eng. Des.* 83 (2008) 771–783.
- [4] S. Smolentsev, R. Moreau, L. Bühler, C. Mistrangelo, MHD thermofluid issues of liquid-metal blankets: phenomena and advances, *Fusion Eng. Des.* 85 (2010) 1196–1205.
- [5] S. Smolentsev, N. Vetcha, M. Abdou, Effect of a magnetic field on stability and transitions in liquid breeder flows in a blanket, *Fusion Eng. Des.* 88 (2013) 607–610.
- [6] S. Sukoriansky, D. Klaiman, H. Branover, E. Greenspan, MHD enhancement of heat transfer and its relevance to fusion reactor blanket design, *Fusion Eng. Des.* 8 (1989) 277–282.
- [7] S. Malang, P. Leroy, G. Casini, R. Mattas, Y. Strebkov, Crucial issues on liquid metal blanket design, *Fusion Eng. Des.* 16 (1991) 95–109.
- [8] I.R. Kirillov, C.B. Reed, L. Barleon, K. Miyazaki, Present understanding of MHD and heat transfer phenomena for liquid metal blankets, *Fusion Eng. Des.* 27 (1995) 553–569.
- [9] M.A. Hossain, Viscous and Joule heating effects on MHD free convection flow with variable plate temperature, *Int. J. Heat Mass Transf.* 35 (1992) 3485–3487.
- [10] J. Sommeria, R. Moreau, Why, how, and when, MHD turbulence becomes two-dimensional, *J. Fluid Mech.* 118 (1982) 507–518.
- [11] P. Davidson, The role of angular momentum in the magnetic damping of turbulence, *J. Fluid Mech.* 336 (1997) 123–150.
- [12] H. Branover, A. Eidelman, M. Nagorny, Use of turbulence modification for heat transfer enhancement in liquid metal blankets, *Fusion Eng. Des.* 27 (1995) 719–724.
- [13] M. Frank, L. Barleon, U. Müller, Visual analysis of two-dimensional magnetohydrodynamics, *Phys. Fluids* 13 (2001) 2287–2295.
- [14] R. Klein, A. Pothérat, Appearance of three dimensionality in wall-bounded MHD flows, *Phys. Rev. Lett.* 104 (2010) 034502.
- [15] D. Krasnov, O. Zikanov, T. Boeck, Numerical study of magnetohydrodynamic duct flow at high Reynolds and Hartmann numbers, *J. Fluid Mech.* 704 (2012) 421.
- [16] N. Kanaris, X. Albets, D. Grigoriadis, S. Kassinos, Three-dimensional numerical simulations of magnetohydrodynamic flow around a confined circular cylinder under low, moderate, and strong magnetic fields, *Phys. Fluids* 25 (2013) 074102.
- [17] A.H.A. Hamid, W.K. Hussam, A. Pothérat, G.J. Sheard, Spatial evolution of a quasi-two-dimensional Kármán vortex street subjected to a strong uniform magnetic field, *Phys. Fluids* 27 (2015) 053602.
- [18] L. Bühler, Instabilities in quasi-two-dimensional magnetohydrodynamic flows, *J. Fluid Mech.* 326 (1996) 125–150.
- [19] A. Pothérat, J. Sommeria, R. Moreau, An effective two-dimensional model for MHD flows with transverse magnetic field, *J. Fluid Mech.* 424 (2000) 75–100.
- [20] A. Pothérat, Quasi-two-dimensional perturbations in duct flows under transverse magnetic field, *Phys. Fluids* 19 (2007) 074104.
- [21] O.G.W. Cassells, T. Vo, A. Pothérat, G.J. Sheard, From three-dimensional to quasi-two-dimensional: transient growth in magnetohydrodynamic duct flows, *J. Fluid Mech.* 861 (2019) 382–406.
- [22] H. Huang, B. Li, Heat transfer enhancement of MHD flow by conducting strips on the insulating wall, *J. Heat Transf.* 133 (2011) 021902.
- [23] W.K. Hussam, M.C. Thompson, G.J. Sheard, Dynamics and heat transfer in a quasi-two-dimensional MHD flow past a circular cylinder in a duct at high Hartmann number, *Int. J. Heat Mass Transf.* 54 (2011) 1091–1100.
- [24] W.K. Hussam, G.J. Sheard, Heat transfer in a high Hartmann number MHD duct flow with a circular cylinder placed near the heated side-wall, *Int. J. Heat Mass Transf.* 67 (2013) 944–954.
- [25] D. Chatterjee, S.K. Gupta, MHD flow and heat transfer behind a square cylinder in a duct under strong axial magnetic field, *Int. J. Heat Mass Transf.* 88 (2015) 1–13.
- [26] O.G.W. Cassells, W.K. Hussam, G.J. Sheard, Heat transfer enhancement using rectangular vortex promoters in confined quasi-two-dimensional magnetohydrodynamic flows, *Int. J. Heat Mass Transf.* 93 (2016) 186–199.
- [27] S.J. Yang, Numerical study of heat transfer enhancement in a channel flow using an oscillating vortex generator, *Heat Mass Transf.* 39 (2003) 257–265.
- [28] W.S. Fu, B.H. Tong, Numerical investigation of heat transfer characteristics of the heated blocks in the channel with a transversely oscillating cylinder, *Int. J. Heat Mass Transf.* 47 (2004) 341–351.
- [29] W.K. Hussam, M.C. Thompson, G.J. Sheard, Enhancing heat transfer in a high Hartmann number magnetohydrodynamic channel flow via torsional oscillation of a cylindrical obstacle, *Phys. Fluids* 24 (2012) 113601.
- [30] A.H.A. Hamid, W.K. Hussam, G.J. Sheard, Heat transfer augmentation of a quasi-two-dimensional MHD duct flow via electrically driven vortices, *Numer. Heat Transf.* 70 (2016) 847–869.
- [31] A.H.A. Hamid, W.K. Hussam, G.J. Sheard, Combining an obstacle and electrically driven vortices to enhance heat transfer in a quasi-two-dimensional MHD duct flow, *J. Fluid Mech.* 792 (2016) 364–396.
- [32] T. Alam, R.P. Saini, J.S. Saini, Use of turbulators for heat transfer augmentation in an air duct—a review, *Renew. Energy* 62 (2014) 689–715.
- [33] R. Karwa, Experimental studies of augmented heat transfer and friction in asymmetrically heated rectangular ducts with ribs on the heated wall in transverse, inclined, V-continuous and V-discrete pattern, *Int. Commun. Heat Mass Transf.* 30 (2003) 241–250.
- [34] J.L. Bhagoria, J.S. Saini, S.C. Solanki, Heat transfer coefficient and friction factor correlations for rectangular solar air heater duct having transverse wedge shaped rib roughness on the absorber plate, *Renew. Energy* 25 (2002) 341–369.

- [35] W.K. Hussam, A.H.A. Hamid, Z.Y. Ng, G.J. Sheard, Effect of vortex promoter shape on heat transfer in MHD duct flow with axial magnetic field, *Int. J. Therm. Sci.* 134 (2018) 453–464.
- [36] U. Burr, L. Barleon, K. Mack, U. Müller, The effect of horizontal magnetic field on liquid metal Rayleigh–Benard convection, FZKA-Report No. 6277, Karlsruhe, 1999.
- [37] L. Barleon, U. Burr, K.J. Mack, R. Stieglitz, Heat transfer in liquid metal cooled fusion blankets, *Fusion Eng. Des.* 51–52 (2000) 723–733.
- [38] N.B. Morley, S. Smolentsev, L. Barleon, I.R. Kirillov, M. Takahashi, Liquid magnetohydrodynamics – recent progress and future directions for fusion, *Fusion Eng. Des.* 51–52 (2000) 701–713.
- [39] R.J. Lingwood, T. Alboussiere, On the stability of the Hartmann layer, *Phys. Fluids* 11 (1999) 2058–2068.
- [40] T.L. Bergman, A.S. Lavine, F.P. Incropera, D.P. DeWitt, *Fundamentals of Heat and Mass Transfer*, John Wiley & Sons, USA, 2007.
- [41] G.E. Karniadakis, M. Israeli, S.A. Orszag, High-order splitting methods for the incompressible Navier–Stokes equations, *J. Comput. Phys.* 97 (1991) 414–443.
- [42] G.E. Karniadakis, S. Sherwin, *Spectral/hp Element Methods for Computational Fluid Dynamics*, Oxford University Press, Britain, 2013.
- [43] G.J. Sheard, Wake stability features behind a square cylinder: focus on small incidence angles, *J. Fluids Struct.* 27 (2011) 734–742.
- [44] W.K. Hussam, M.C. Thompson, G.J. Sheard, Optimal transient disturbances behind a circular cylinder in a quasi-two-dimensional magnetohydrodynamic duct flow, *Phys. Fluids* 24 (2012) 024105.
- [45] S. Smolentsev, C. Wong, S. Malang, M. Dagher, M. Abdou, MHD considerations for the DCLL inboard blanket and access ducts, *Fusion Eng. Des.* 85 (2010) 1007–1011.
- [46] B. Schulz, Thermophysical properties of the Li (17) Pb (83) alloy, *Fusion Eng. Des.* 14 (1991) 199–205.
- [47] E.M. de les Valls, L.A. Sedano, L. Batet, I. Ricapito, A. Aiello, O. Gastaldi, F. Gabriel, Lead–lithium eutectic material database for nuclear fusion technology, *J. Nucl. Mater.* 376 (2008) 353–357.